Modeling of three-dimensional exciplex pumped fluid Cs vapor laser with transverse and longitudinal gas flow

Chenyi Su[1], Xingqi Xu[1,2*], Jinghua Huang[1] and Bailiang Pan[1*]

[1]Department of Physics, Zhejiang University, Hangzhou, 310027, China
[2]Interdisciplinary Center for Quantum Information, State Key Laboratory of Modern Optical Instrumentation, and Zhejiang Province Key Laboratory of Quantum Technology and Device, Department of Physics, Zhejiang University, Hangzhou 310027, Zhejiang Province, China

Abstract Considering the thermodynamical fluid mechanics in the gain medium and laser kinetic processes, a three-dimensional theoretical model of exciplex pumped Cs vapor laser with longitudinal and transverse gas flow is established. The slope efficiency of laser calculated by the model shows good agreement with the experimental data. The comprehensive three-dimensional distribution of temperature and particle density of Cs is depicted. The influence of pump intensity, wall temperature and fluid velocity on the laser output performance are also simulated and analyzed in detail, suggesting that a higher wall temperature can guarantee a higher output laser power while causing a more significant heat accumulation in the cell. Compared to longitudinal gas flow, the transverse flow can improve the output laser power by effectively removing the generated heat accumulation and alleviating the temperature gradient in the cell.

Key words: excimer lasers; gas flow; simulation; theoretical model

I. INTRODUCTION

Since the first realization of Ti: Sapphire pumped Rb vapor laser operating on the resonance at 795 nm by Krupke et al. in 2003[1], diode-pumped alkali vapor laser (DPAL) has become a research focus in high-power laser field due to its good beam quality with high output power and efficient energy conversion with excellent thermal management[2-7]. However, the huge spectral mismatch between the pump line of commercial semiconductors and the absorption line of alkali atoms becomes a non-negligible issue encountered in the development of DPAL[8]. A new class of laser device, exciplex pumped alkali vapor laser (XPAL), was invented for throughout resolving such a problem. XPAL was first experimentally reported by Readle et al. in 2008[9] while the idea can be dated to 2002[10]. The kinetic processes and lasing properties of XPAL significantly differ from DPAL as the intermedium energy states introduced by the buffer gas not only broadens the atomic resonance line to nanometers but also directly takes part in the optically pump process, promising an efficient use of pump power[9, 11]. Because of these advantages, Palla and Carroll et al. extended the theoretical studies in details [11-15], in which the operating mechanism and output performance of XPALs were simulated and predicted, respectively. Until now, four-level and five-level XPALs with Cs-Ar, Cs-Kr, Cs-Xe and Rb-Kr as gain medium have been realized in experiments[9, 16-19]. However, a sharp radial temperature gradient caused by severe thermal effects will occur in the gain medium during an CW operation XPAL, resulting in an uneven distribution of the number density of Cs particles, thereby reducing the output power of laser[20]. To solve this issue, on the one hand, multi-pulse pump can be used instead of CW pump to alleviate the heat loading[21, 22]; On the other hand, studies show that longitudinal gas flow of sonic-level is required to control the thermal accumulation in a CW XPAL[23-25], which is difficult to realize in experiment.

In this paper, combined rate equations, heat conduction equations and fluid heat transfer equations, a three-dimensional XPCsL model is established to study more effective methods on heat dissipation. The effect of pump intensity, wall temperature, directions and velocity of gas flow on laser output performance are simulated and analyzed, where the three-dimensional distribution of temperature and particle number density of Cs are presented in detail.

II. Description of model

The schematic diagram of the XPAL device is shown in Fig. 1. Transverse and longitudinal gas flow XPAL systems are depicted in Fig. 1(a) and Fig. 1(b), respectively, where the pump light is introduced by PBS and oscillates in the resonant cavity formed by output coupler (OC) and high reflector (HR), and the Cs-Ar mixed gas is filled in a circulating flow structure. As can be seen in Fig. 1(c), the cell is divided into small cuboids having a length, width and height of $\Delta x \times \Delta y \times \Delta z$. Regarded as Gaussian beams, the radius of pump and laser beam in the z-axis direction and the light intensity distribution of them on the x-y plane are described by $w_{p,l}(z)$ and $f_{p,l}(x,y,z)$, respectively.

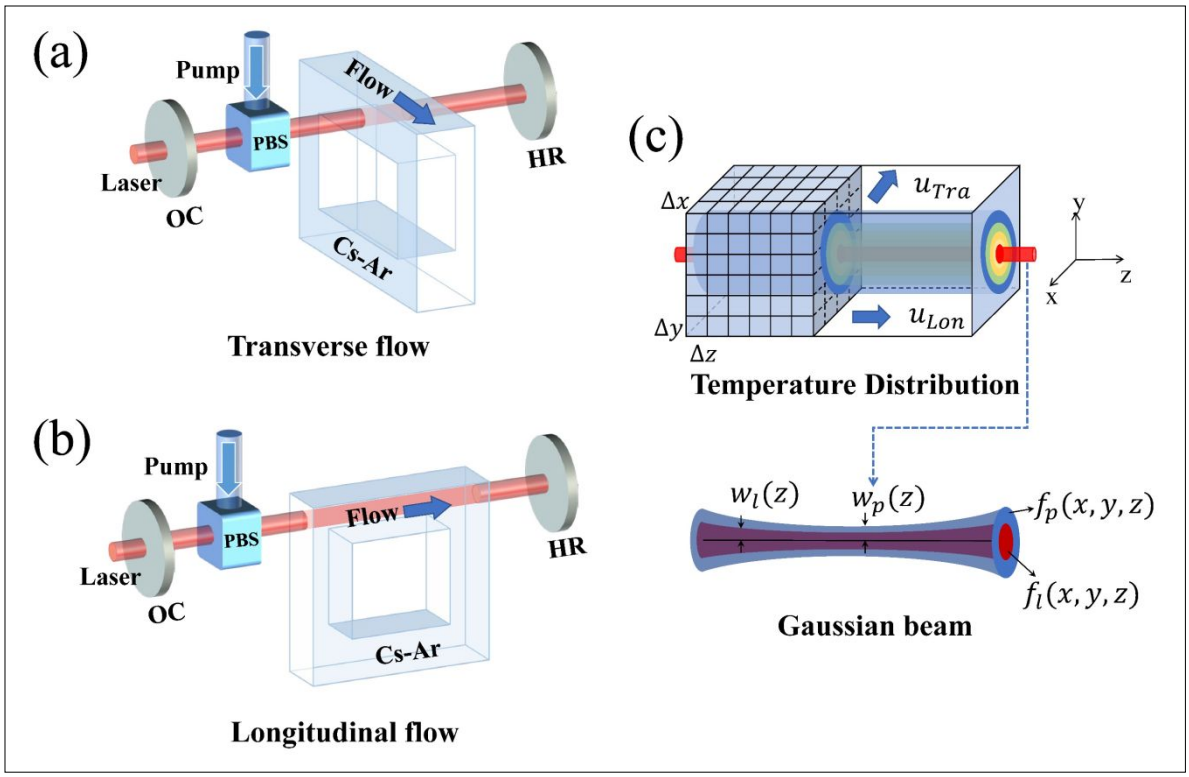

Fig. 1 Sketch of optical systems of XPCsL.

2.1 kinetic processes of XPAL

The kinetic processes involved in the simulation are presented in Fig. 2. The rate equations in each volume element can be written as follows:

$$\frac{dn_1(x,y,z)}{dt} = k_{01}n_0(x,y,z)[Ar] - k_{10}n_1(x,y,z) - P_{12}(x,y,z), \tag{2}$$

$$\frac{dn_2(x,y,z)}{dt} = P_{12}(x,y,z) - k_{23}n_2(x,y,z) + k_{32}n_3(x,y,z)[Ar], \tag{3}$$

$$\begin{aligned}\frac{dn_3(x,y,z)}{dt} = &-L_{30}(x,y,z) + k_{23}n_2(x,y,z) - k_{32}n_3(x,y,z)[Ar] + A_{43}(x,y,z) \\ &- A_{30}(x,y,z) - Ep_{34}(x,y,z) - Phe_{34}(x,y,z) - Pen(x,y,z),\end{aligned} \tag{4}$$

$$\begin{aligned}\frac{dn_4(x,y,z)}{dt} = &Ep_{34}(x,y,z) - Pen(x,y,z) - A_{43}(x,y,z) \\ &+ R_2(x,y,z) - Phi_{45}(x,y,z) + Phe_{34}(x,y,z),\end{aligned} \tag{5}$$

$$\frac{dn_5(x,y,z)}{dt} = Phi_{45}(x,y,z) + Pen(x,y,z) - R_1(x,y,z), \tag{6}$$

$$\frac{dn_6(x,y,z)}{dt} = R_1(x,y,z) - R_2(x,y,z), \tag{7}$$

$$\frac{dn_0(x,y,z)}{dt} = N_{Cs}(x,y,z) - \sum_{i=1}^{i=6} n_i(x,y,z), \tag{8}$$

where $n_i(i=0,1,2,3,4,5,6)$ denotes the population densities of energy states, subscripts of 0 – 6 represent different atomic states including atomic ground state, $6^2S_{1/2}$, excimer ground state, $X^2\Sigma_{1/2}^+$, excimer excited state, $B^2\Sigma_{1/2}^+$, atomic D2 states, $6^2P_{3/2}$, atomic higher excited states, $6^2D_{3/2,5/2}(8^2S_{1/2})$, ionized ground state, Cs^+ and associative state, Cs_2^+, respectively. $N_{Cs}(x,y,z) = n_{CS}T_w / T(x,y,z)$ denotes density of Cs vapor at the temperate of $T(x,y,z)$, and n_{Cs} is the total density of Cs at T_w. $k_{ij}(i,j=0,1,2,3)$ are the thermal equilibrium constants between the energy levels.

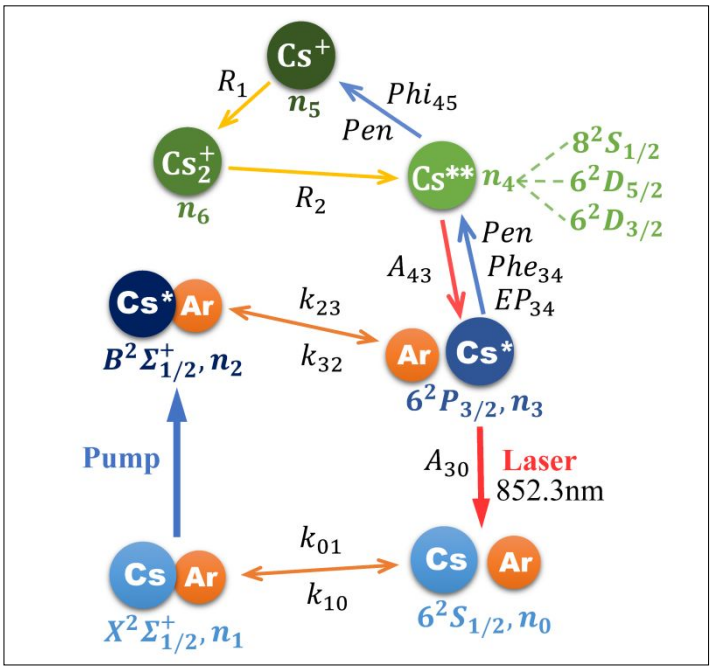

Fig. 2 Diagram of energy states in high-power XPCsL system

The rates of laser emission L_{30} and pump absorption P_{12} are formulated as

$$L_{30}(x,y,z) = [n_3(x,y,z) - 2n_0(x,y,z)]\sigma_{D1} \cdot \frac{f_l(x,y,z)[P_l^+(x,y,z) + P_l^-(x,y,z)]}{h\nu_l}, \tag{9}$$

$$P_{12}(x,y,z) = [n_1(x,y,z) - n_2(x,y,z)] \cdot \int \frac{\sigma_{D2}(\nu) f_p(x,y,z) P_p(x,y,z,\nu)}{h\nu_p} d\nu, \quad (10)$$

where σ_{D2} is the spectrally resolved atomic absorption cross-section and σ_{D1} is the stimulated emission cross-section.

The pump beam at *z=0* is described as:

$$P_p(x,y,0,\nu) = P_{p,0} \frac{2}{\nu_p} \sqrt{\frac{\ln 2}{\pi}} \exp\left[-4 \ln 2 \frac{(\nu - \nu_p)^2}{\Delta \nu_p{}^2} \right], \quad (11)$$

where ν_p and $\Delta\nu_p$ are the central frequency and the FWHM of the pump beam, respectively. $p_{p,0}$ denotes the pumping power in total. f_p and f_l depict the light intensity distribution of the pump and laser beam in (x, y, z), written as

$$f_{p,l}(x,y,z) = \frac{\sqrt{2}}{\pi w_{p,l}(z)^2} \exp\left\{ -\sqrt{2} \left[\frac{x^2 + y^2}{w_{p,l}(z)^2} \right] \right\}, \quad (12)$$

where $w_p(z)$ and $w_l(z)$ are the radii of pump and laser beam at z,

$$w_{p,l}(z) = w_{0,p,l} \sqrt{\left[\frac{(z - z_{0,p,l}) \lambda_{p,l}}{\pi w_{0,p,l}} \right]^2 + 1}, \quad (13)$$

where $z_{0,p,l}$ are the z-coordinates of the pump and laser beam waists ($w_{0,p,l}$).

The other parameters involved in the rate equations are listed in Table 1.

Table 1. Kinetic processes in the XPAL system.

No.	Process	Cross Section/Rate	References
	Thermal associative/ dissociative process		
1	$Cs(6^2S_{1/2}) + Ar \; f \; Cs(X^2\Sigma^+_{1/2})Ar$	k_{01}, k_{10}	[12]
2	$Cs(B^2\Sigma^+_{1/2})Ar + Ar \; f \; Cs(6^2P_{3/2}) + Ar$	k_{23}, k_{32}	
	Pumping		
3	$Cs(X^2\Sigma^+_{1/2})Ar + h\nu_p \rightarrow Cs(B^2\Sigma^+_{1/2})Ar$	P_{12}	Eq. (9)
	Lasing		
4	$Cs(6^2P_{3/2}, 6^2P_{1/2}) \rightarrow Cs(6^2S_{1/2}) + h\nu_l$	L_{30}	Eq. (8)
	Spontaneous emission		
5	$Cs(6^2P_{3/2}) \rightarrow Cs(6^2S_{1/2}) + h\nu_l$	A_{30}	[26]

6	$Cs(6^2D_{3/2}, 6^2D_{5/2}) \rightarrow Cs(6^2P_{3/2}) + h\nu$	A_{43}	
	Photoexcitation		
7	$Cs(6^2P_{3/2}, 6^2P_{1/2}) + h\nu_p(h\nu_l) \rightarrow Cs(6^2D_{3/2,5/2}, 8^2S_{1/2})$	Phe_{34}	[26]
	Energy pooling		
8	$2Cs(6^2P_{3/2}, 6^2P_{1/2}) \rightarrow Cs(6^2D_{3/2,5/2}, 8^2S_{1/2}) + Cs(6^2S_{1/2})$	Ep_{34}	[27]
	Photoionization		
9	$Cs(6^2D_{3/2,5/2}, 8^2S_{1/2}) + h\nu_{p,l} \rightarrow Cs^+ + e$	Phi_{45}	[27]
	Penning ionization		
10	$Cs(6^2D_{3/2,5/2}, 8^2S_{1/2}) + Cs(6^2P_{3/2,1/2}) \rightarrow Cs^+ + Cs(6^2S_{1/2}) + e$	Pen	[27]
	Dissociative recombination		
11	$Cs^+ + Cs(6^2S_{1/2}) + Cs \rightarrow Cs_2^+ + Cs$	R_1	[26]
12	$Cs^+ + Cs(6^2S_{1/2}) + Ar \rightarrow Cs_2^+ + Ar$		
13	$Cs_2^+ + e \rightarrow Cs(6^2D_{3/2,5/2}, 8^2S_{1/2}) + Cs(6^2S_{1/2})$	R_2	

2.2 Solution for laser power

The propagations of laser and pump lights along the z-axis are described by the following iterative equations:

$$P_p(x,y,z+\Delta z) = P_p(x,y,z) \cdot \sum_S f_p(x,y,z) \exp\left\{-[n_1(x,y,z) - n_2(x,y,z)]\sigma_{D2}(\nu)\Delta z\right\}\Delta x\Delta y, \tag{14}$$

$$P_l^{\pm}(x,y,z+\Delta z) = P_l^{\pm}(x,y,z) \cdot \sum_S f_l(x,y,z) \exp\left\{\pm[n_3(x,y,z) - 2n_0(x,y,z)]\sigma_{D1}\Delta z\right\}\Delta x\Delta y, \tag{15}$$

where S is the cross-section of the cell.

The initial boundary conditions of P_l^+ and P_l^- at $z=0$ are given by:

$$P_l^-(0) = P_l / \left[T_l(1-R_{oc})\right], \tag{16}$$

$$P_l^+(0) = P_l T_l R_{oc} / (1-R_{oc}). \tag{17}$$

To calculate the output power of laser, we first assume a laser output power value and then substitute it into the initial equation at $z=0$ for iterative operation. If the boundary equation $P_l^-(l) = P_l^+(l) T_l^2 T_s^2 R_p$ at $z=L$ is satisfied, the correct output laser power is obtained, where R_{oc} and R_p are the reflectivity of the output coupler and the back reflector. T_l is the single-pass cell window transmission and T_s is the intra-cavity single-pass loss.

2.3 Calculation of temperature distribution

The heat generated by multiple transitions in each volume element is given by

$$\begin{aligned}\Omega(x,y,z) = \Delta x\Delta y\Delta z[&(k_{01}n_0(x,y,z)[Ar]-k_{10}n_1(x,y,z))\Delta E_{10} \\ &+(-k_{32}n_3(x,y,z)[Ar]+k_{23}n_2(x,y,z))\Delta E_{23}+R_2(x,y,z)E_{io}]\end{aligned} \tag{18}$$

where ΔE denotes the energy gap of the corresponding levels and E_{io} is the ionization energy.

2.3.1 temperature distribution without medium flow

The heat dissipation in the cell is mainly attributed to heat conduction when *u=0*, which can be expressed as

$$H_c(x,y,z) = 2\pi\Delta z\frac{k_e[T(x,y,z)-T_w]}{\ln(R/\sqrt{x^2+y^2})}, \tag{19}$$

where k_e is the effective thermal conductivity[28] and *R* is the radius of cell. $T(x,y,z)$ can be obtained by the heat balance $\Omega(x,y,z) = H_c(x,y,z)$.

2.3.2 temperature distribution with medium flow

The heat removed in each volume by flowed gases with different direction can be calculated by

$$F_L(x,y,z)=\begin{cases}\dfrac{u\Delta x\Delta y n_t(x,y,z)}{N_A}\displaystyle\int_{T_w}^{T(x,y,z)}C_p(T')dT', z=0\\ \dfrac{u\Delta x\Delta y n_t(x,y,z)}{N_A}\displaystyle\int_{T(x,y,z-\Delta z)}^{T(x,y,z)}C_p(T')dT', z>0\end{cases} \tag{20}$$

$$F_T(x,y,z)=\begin{cases}\dfrac{u\Delta z\Delta y n_t(x,y,z)}{N_A}\displaystyle\int_{T_w}^{T(x,y,z)}C_p(T')dT', \mathrm{x}=0\\ \dfrac{u\Delta z\Delta y n_t(x,y,z)}{N_A}\displaystyle\int_{T(x-\Delta x,y,z)}^{T(x,y,z)}C_p(T')dT', \mathrm{x}>0\end{cases} \tag{21}$$

where $R_L(x,y,z)$ and $F_T(x,y,z)$ denote the heat removed by longitudinal flow and transverse flow, respectively. *u* and n_t are the velocity and number density of the total mixed gases. $C_P(T)$ is the average molar heat capacity of the mixed gases.

On the other hand, the heat transferred by heat conduction in each volume element can be written as

$$\Phi(x,y,z) = K(x,y,z)Nu(x,y,z)$$
$$\cdot\{\frac{\Delta x\Delta y}{\Delta z}\{[T(x,y,z+\Delta z)-T(x,y,z)]-[T(x,y,z)-T(x,y,z-\Delta z)]\}$$
$$+\frac{\Delta y\Delta z}{\Delta x}\{[T(x+\Delta x,y,z)-T(x,y,z)]-[T(x,y,z)-T(x-\Delta x,y,z)]\} \quad (22)$$
$$+\frac{\Delta z\Delta x}{\Delta y}\{[T(x,y+\Delta y,z)-T(x,y,z)]-[T(x,y,z)-T(x,y-\Delta y,z)]\}\},$$

where K and Nu are the thermal conductivity and Nusselt number[28], respectively.

Then the temperature $T(x,y,z)$ in each volume element can be obtained from the following balance equation:

$$\Omega(x,y,z) = F_{L,T}(x,y,z) + \Phi(x,y,z) \quad (23)$$

III. Results and discussion

3.1 Comparison with experimental result

Figure 3 is the comparison of slope efficiency between experiment[19] (a) and simulation (b) results with the parameters in Table 2. A laser pulse train with FWHM of 40 ns is used in experiment, generating a $\sim 10^4$ W of peak power for optical pump. Good agreement between simulation and experiments can be seen at the slope efficiency.

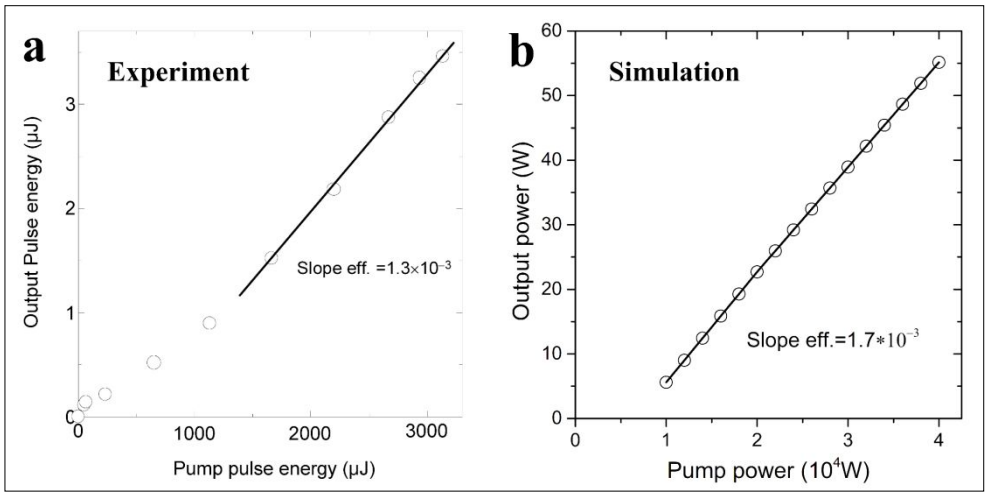

Fig. 3 Comparison of slope efficiency between experiment[19] and simulation results.

Table 2. Parameters of experiment and simulation.

Length of cell	Temperature	Pressure of Ar	OC ratio
4 cm	455 K	1270 Torr	0.13

3.2 Three-dimensional distribution of temperature

The temperature distribution in the gain medium can highly influence the output performance especially on the beam quality. Figure 4 presents the three-dimensional distribution of temperature in the cell under conditions of longitudinal and transverse gas flow, where the velocity of flow and wall temperature are both set at 50 m/s and 473 K, respectively. As shown in Fig. 4 (a), the temperature distribution is circularly distributed and outward diffuses while that is elliptically outward distributed in Fig. 4 (b). The maximum temperature in (a) and (b) are 831.4 K and 495.9 K, indicating an advantage that transverse flow can take in temperature control. On the other hand, compared Fig. 4 (a) to (b), one can note that the maximum point of temperature in the x-y plane is shifted from (0, 0) of coordinate to (0.7, 0) when the cooling flow is changed from longitudinal to transverse. Therefore, though the longitudinal gas flow can effectively reduce the temperature overall, it also creates a new temperature gradient in the z-axis direction, while the transverse flow avoids this problem by moving the majority of heat away from the optical axis. In general, the transverse gas flow can more effectively control the paraxial temperature, so that improving the operating environment of laser system.

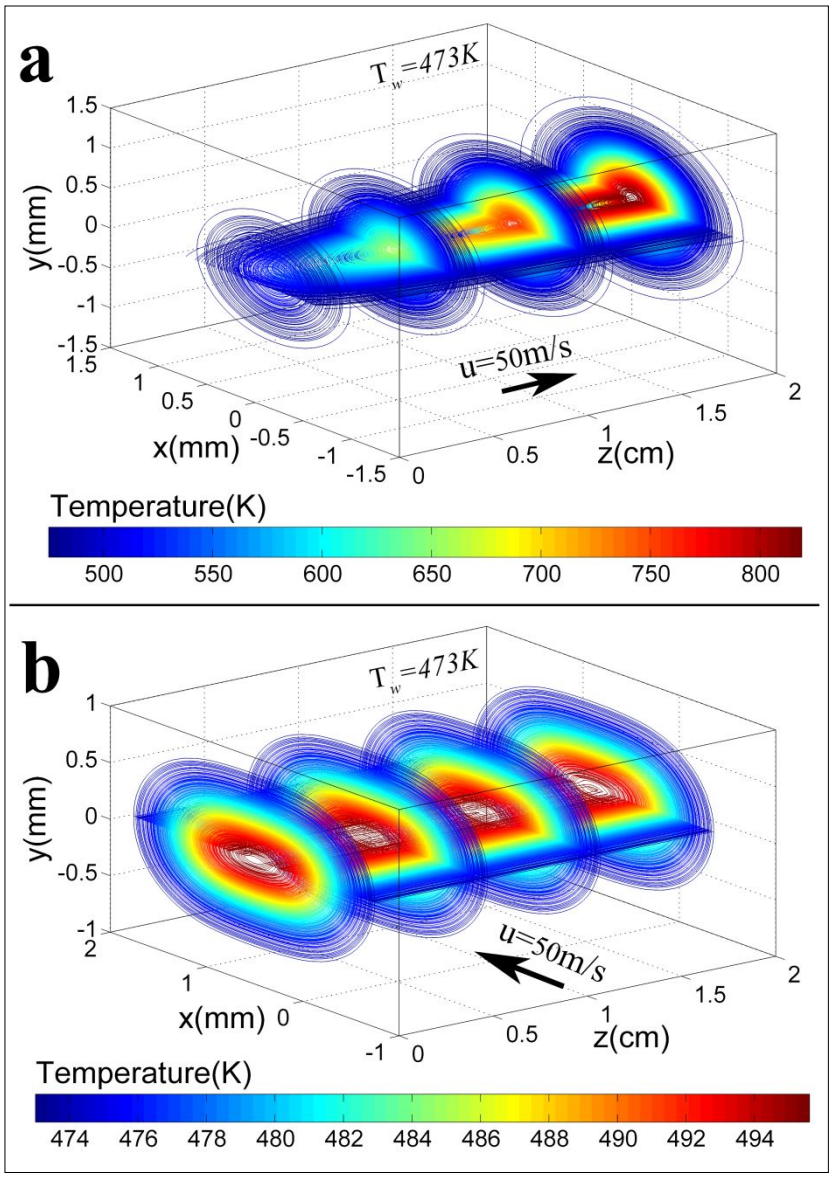

Fig. 4 Three-dimensional temperature distribution under different flow directions. The velocity of flow and wall temperature in (a) and (b) are 50 m/s and 473 K.

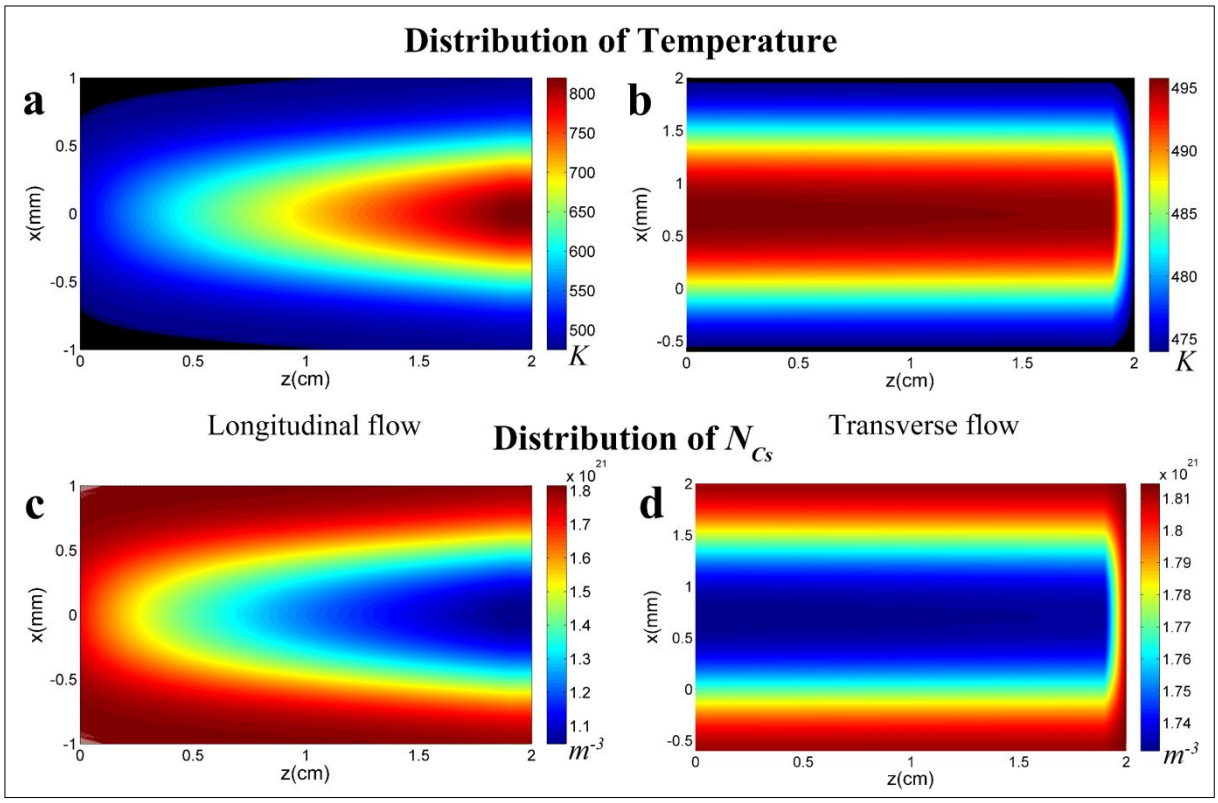

Fig. 5 (a), (b): The temperature distribution in the x-y plane at y=0 in Fig. 4 (a) and (b);

(c), (d): The distribution of N_{Cs} in the x-y plane at y=0 in Fig. 4 (a) and (b).

Figure 5 shows the more detailed distribution of temperature and N_{Cs} on the *x-z* plane at *y=0* in Fig. 4. The gas flow is longitudinal in (a), (c) and transverse in (b), (d). As $N_{Cs}(x,y,z) = n_{CS}T_w(x,y,z)/T(x,y,z)$, it can be seen from the comparison between the upper and lower graphs that the particle number densities are relatively lower in aera with high temperatures, resulting in a decay of output performance. The lowest N_{Cs} in Fig. 5 (c) and (d) are $1.0469\times10^{21}\ m^{-3}$ and $1.7313\times10^{21}\ m^{-3}$, respectively. Moreover, the particle number density around the optical axis in (d) is less affected. As a result, with $u = 50\,m/s$, $T_w = 473K$, and $I_P = 4.5\times10^6\ W/cm^2$, the optical-to-optical efficiency is 2.05% under transverse gas flow while that is 1.23% under longitudinal gas flow, proving the former can improve the laser output performance of a XPCsL.

3.3 The influence of flow on optical-to-optical efficiency.

In section 3.2, we confirm that the temperature distribution in the gain medium can affect the output performance of the laser by changing distribution of the number density of Cs particles. Therefore, in this section, we will take the maximum temperature as an indicator to characterize the temperature gradient in the cell, and further study the influences of pump intensity, wall temperature and gas flows with different directions and velocities on the optical-to-optical efficiency. The parameters used in the simulation are listed in Table. 3.

Table. 3 Parameters used in the simulation

Parameters	Definition	Value
L	Length of the cell	2 cm
S	Cross section of the cell	2 mm × 2 mm
P_{Ar}	Pressure of ethane	1300 Torr
R_{oc}	Output coupler reflectivity	0.5
R_p	back mirror reflectivity	0.99
T_l	Single-pass cell window transmission	0.98
T_s	Intra-cavity single-pass loss	0.9
$w_{0,p}$	Waist of the pump beam	0.5 mm
$w_{0,l}$	Waist of the laser beam	0.5 mm

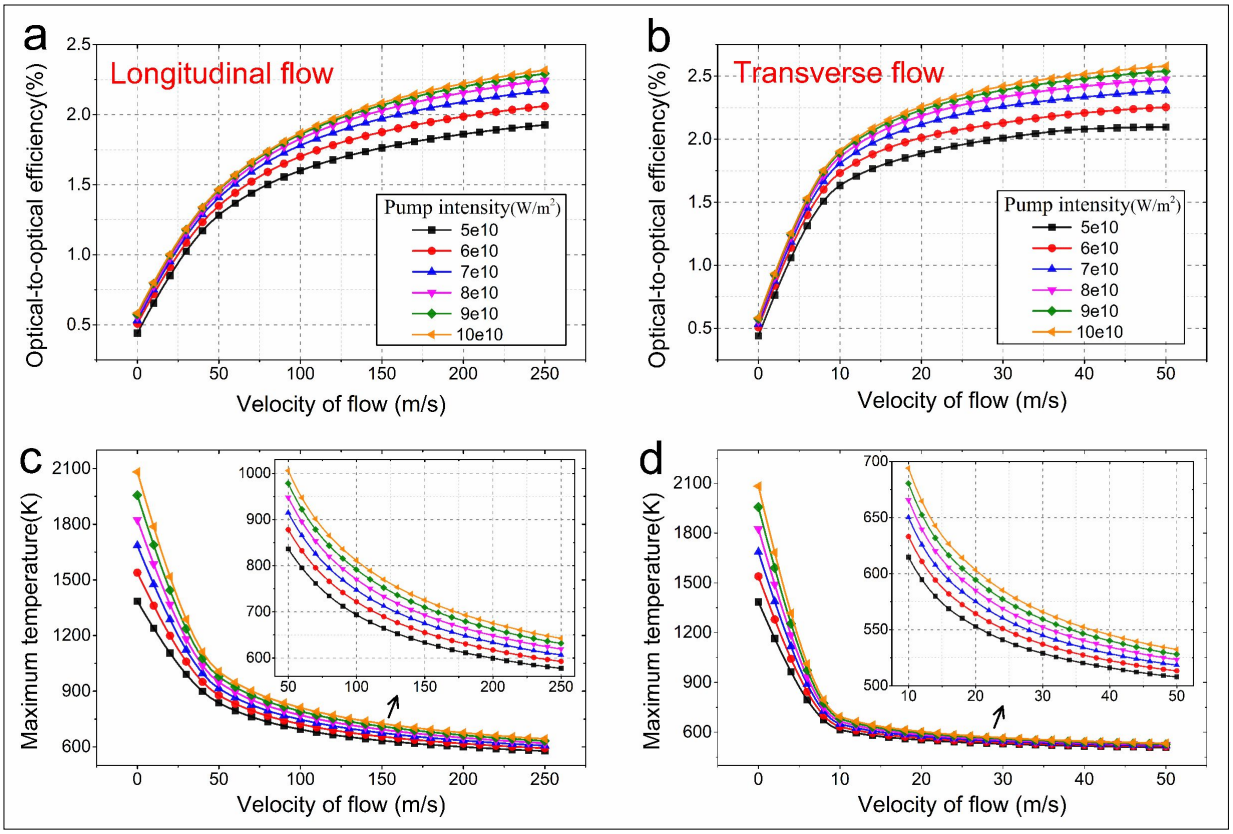

Fig. 6 Optical-to-optical efficiency and maximum temperature as a function of flow velocity with different pump intensity at $T_w = 473K$.

Figure 6 depicts the optical-to-optical efficiency and maximum temperature as a function of flow velocity with different pump intensity at $T_w = 473K$. One can see from Fig. 6 that severe heat accumulation will occur in the gain medium during the operation without gas flow, which greatly limits the output performance of laser. The optical-to-optical efficiency in Fig. 6 (a) and (b) increases with the rise of flow velocity and pump intensity, and then tends to be saturated, while the maximum temperature in Fig. 6 (c) and (d) is the opposite. In the case of longitudinal gas flow, in the range of (0, ~50) m/s, the maximum temperature and optical-to-optical efficiency are more sensitive to the change of fluid velocity, while that range in Fig. 6 (b) and (d) is (0, ~10) m/s. Especially in Fig. 6 (d), the effect of the fluid velocity on the temperature gradient in the gain medium is relatively small after it crossing 20 m/s. Furthermore, the laser output tends to be

saturated with a transverse gas flow of ~50 m/s, while ~250 m/s of longitudinal gas flow is needed in the same situation.

On the other hand, compared with Fig. 6 (a) and (c), the slope of the curve in Fig. 6 (b) and (d) are larger, respectively, indicating that the transverse gas flows have a better heat dissipation efficiency. In addition, under the same conditions, the maximum temperature in the cell is always lower with transverse gas flow, resulting in a higher laser output.

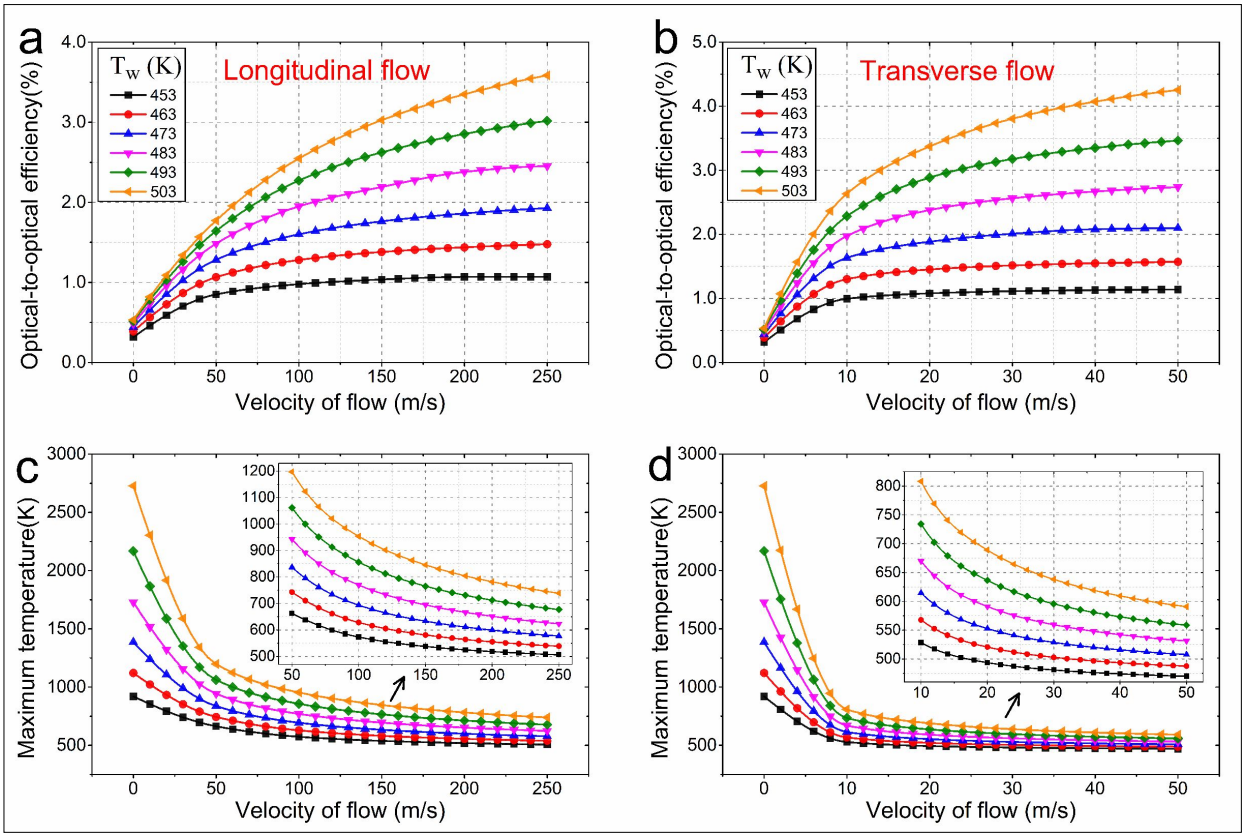

Fig. 7 Optical-to-optical efficiency and maximum temperature as a function of flow velocity with different wall temperature at pump intensity $= 5\times10^{10}\ W/m^2$.

The relationship between optical-to-optical efficiency and velocity of flow with different wall temperature at pump intensity $=5\times10^{10}\ W/m^2$ is plotted in Fig. 7, in which the conclusions obtained in Figure 6 can also be confirmed. Besides, the maximum temperature in Fig. 7 rises higher than that in Fig. 6 when $u=0$ as the wall temperature increases. In other words, a higher

wall temperature is more likely to generate a larger heat load in the gain medium. In the case of $u>0$, the slope of curve representing the maximum temperature decreases significantly after the fluid velocity in Fig.7 (c) and (d) reaches ~100 m/s and ~20 m/s, respectively. Compared Fig. 7 (a) and (b) with Fig. 6 (a) and (b), it can be concluded that the wall temperature has a greater contribution to the improvement of optical-to-optical efficiency than the pump intensity. At the same time, a higher wall temperature means a faster velocity of flow is required to reach the saturation value of the laser output, which is shown in Fig. 7 (a) and (b): with wall temperature higher than 503K, longitudinal gas flow of quasi-sonic level and transverse gas flow greater than 50 m/s may be required to alleviate the thermal effect in the cell, maximizing the laser output.

IV. Summary

In this paper, considering the kinetic, heat conduction and fluid dynamics processes in the gain medium, we established a comprehensive three-dimensional physical model to simulate and analysis the laser output performance and temperature distribution in an exciplex pumped Cs vapor laser with longitudinal and transverse gas flow. The slope efficiency of laser calculated by the model is consistent with the experimental results. The three-dimensional distribution of temperature and number density of Cs particles in the cell with different directions of gas flow are simulated and depicted, demonstrating that the transverse gas flow can more effectively and uniformly alleviate the heat accumulation on the optical axis of pump light and laser, resulting in a higher particle number density of Cs in the cell. Furthermore, influences of pump intensity, wall temperature and fluid velocity with different directions on maximum temperature in the cell and optical-to-optical efficiency are presented and analyzed in detail. The results indicated that the optical-to-optical efficiency increases with the pump intensity, wall temperature and flow velocity. Rising the wall temperature can better improve the potential of laser output than rising the pump

intensity. Meanwhile, it will also cause a more significant heat accumulation in the gain medium, where higher speed gas flow is required to alleviate it. On the other hand, compared with the longitudinal gas flow, the transverse gas flow with a lower velocity can more effectively remove the generated heat accumulation and reduce the temperature gradient in the cell to enhance the laser output. This work is of great help in revealing the kinetic and fluid dynamic mechanism and output characteristics in an exciplex pumped Cs vapor laser and promoting the realization of high efficiency fluid XPCsL.

Acknowledgement

This work was supported by the Aerospace Science and Technology Fund under Grant No. KM20170269.

References

1. W. F. Krupke, R. J. Beach, V. K. Kanz, and S. A. Payne, "Resonance transition 795-nm rubidium laser," Opt. Lett. **28**, 2336-2338 (2003).
2. W. F. Krupke, R. J. Beach, V. K. Kanz, and S. A. Payne, *DPAL: a new class of CW near-infrared high-power diode-pumped alkali (vapor) lasers*, Lasers and Applications in Science and Engineering (SPIE, 2004), Vol. 5334.
3. B. Zhdanov and R. Knize, *Diode pumped alkali lasers*, SPIE Security + Defence (SPIE, 2011), Vol. 8187.
4. T. Ehrenreich, B. Zhdanov, T. Takekoshi, S. P. Phipps, and R. J. Knize, "Diode pumped caesium laser," Electronics Letters **41**, 415-416 (2005).
5. B. Zhdanov, C. Maes, T. Ehrenreich, A. Havko, N. Koval, T. Meeker, B. Worker, B. Flusche, and R. J. Knize, "Optically pumped potassium laser," Optics Communications **270**, 353-355 (2007).
6. A. V. Bogachev, S. G. Garanin, A. M. Dudov, V. A. Yeroshenko, S. M. Kulikov, G. T. Mikaelian, V. A. Panarin, V. O. Pautov, A. V. Rus, and S. A. Sukharev, "Diode-pumped caesium vapour laser with closed-cycle laser-active medium circulation," Quantum Electronics **42**, 95-98 (2012).
7. G. Pitz, G. Hager, T. Tafoya, J. Young, G. Perram, and D. Hostutler, *An experimental high pressure line shape study of the rubidium D1 and D2 transitions with the noble gases, methane, and ethane*, SPIE LASE (SPIE, 2014), Vol. 8962.
8. G. A. Pitz, C. D. Fox, and G. P. Perram, "Pressure broadening and shift of the cesium D-2 transition by the noble gases and N-2, H-2, HD, D-2, CH4, C2H6, CF4, and He-3 with comparison to the D-1 transition," Physical Review A **82**, 042502 (2010).
9. J. D. Readle, C. J. Wagner, J. T. Verdeyen, D. L. Carroll, and J. G. Eden, "Lasing in Cs at 894.3 nm pumped by the dissociation of CsAr excimers," in *Electronics Letters,* (Institution of Engineering and Technology, 2008), pp. 1466-1467.
10. R. V. Markov, A. I. Plekhanov, and A. M. Shalagin, "Population Inversion Induced by Collisions in a Two Level System under Nonresonance Optical Excitation," Physical Review Letters **88**, 213601 (2002).
11. A. D. Palla, D. L. Carroll, J. T. Verdeyen, and M. C. Heaven, *XPAL modeling and theory*, SPIE LASE (SPIE, 2011), Vol. 7915.

12. A. D. Palla, D. L. Carroll, J. T. Verdeyen, J. D. Readle, T. M. Spinka, C. J. Wagner, J. G. Eden, and M. C. Heaven, "Multi-Dimensional Modeling of the XPAL System," Proc Spie **7581**(2010).
13. D. L. Carroll, A. D. Palla, and J. T. Verdeyen, *Exciplex pumped alkali laser (XPAL) theory and modeling*, XIX International Symposium on High-Power Laser Systems and Applications (SPIE, 2013), Vol. 8677.
14. A. D. Palla, J. T. Verdeyen, and D. L. Carroll, *Exciplex pumped alkali laser (XPAL) modeling and theory*, 18th International Symposium on Gas Flow and Chemical Lasers and High Power Lasers (SPIE, 2010), Vol. 7751.
15. D. L. Carroll and J. T. Verdeyen, "A simple equilibrium theoretical model and predictions for a continuous wave exciplex pumped alkali laser," Journal of Physics B: Atomic, Molecular and Optical Physics **46**, 025402 (2013).
16. J. D. Readle, J. T. Verdeyen, J. G. Eden, S. J. Davis, K. L. Galbally-Kinney, W. T. Rawlins, and W. J. Kessler, "Cs 894.3 nm laser pumped by photoassociation of Cs-Kr pairs: excitation of the Cs D2 blue and red satellites," Opt. Lett. **34**, 3638-3640 (2009).
17. J. D. Readle, C. J. Wagner, J. T. Verdeyen, D. L. Carroll, and J. G. Eden, *Lasing in alkali atoms pumped by the dissociation of alkali-rare gas exciplexes (excimers)*, SPIE LASE: Lasers and Applications in Science and Engineering (SPIE, 2009), Vol. 7196.
18. A. E. Mironov, D. L. Carroll, J. W. Zimmerman, and J. G. Eden, "Cs D2 line laser (852.1 nm) pumped by the photoassociation of Cs-Ar, Cs-Kr, and Cs-Xe collision pairs: Impact of rare gas partner on threshold and efficiency," Applied Physics Letters **113**, 051105 (2018).
19. M. Endo, T. Nagai, and F. Wani, *Experimental investigation and numerical simulation of exciplex pumped alkali lasers*, XIX International Symposium on High-Power Laser Systems and Applications (SPIE, 2013), Vol. 8677.
20. X. Xu, B. Shen, C. Xia, and B. Pan, "Modeling of Kinetic and Thermodynamic Processes in a Flowing Exciplex Pumped Alkali Vapor Laser," IEEE Journal of Quantum Electronics **53**, 1-7 (2017).
21. C. Su, B. Shen, X. Xu, C. Xia, and B. Pan, "Simulation and analysis of the time evolution of laser power and temperature in static pulsed XPALs," High Power Laser Science and Engineering **7**, e44 (2019).
22. C. Su, X. Xu, J. Huang, and B. Pan, "Numerical simulations on a nanosecond-pulse exciplex pumped cesium vapor laser," Opt. Express **28**, 26302-26312 (2020).
23. X. Xu, B. Shen, J. Huang, C. Xia, and B. Pan, "Theoretical investigation on exciplex pumped alkali vapor lasers with sonic-level gas flow," Journal of Applied Physics **122**, 023304 (2017).
24. X. Xu, B. Shen, J. Huang, C. Xia, and B. Pan, "Detailed computation on exciplex pumped alkali vapor laser with supersonic flow," Opt. Express **25**, 32745-32756 (2017).
25. J. Huang, C. Xia, X. Xu, C. Su, and B. Pan, "Theoretical simulation on exciplex pumped Rb vapor laser," Opt. Express **27**, 132-141 (2019).
26. K. Waichman, B. D. Barmashenko, and S. Rosenwaks, "Computational fluid dynamics modeling of subsonic flowing-gas diode-pumped alkali lasers: comparison with semi-analytical model calculations and with experimental results," J. Opt. Soc. Am. B **31**, 2628-2637 (2014).
27. M. M.A and Y. Gamal, "Effect of energy pooling collisions in formation of a cesium plasma by continuous wave resonance excitation," Optica Applicata **40**(2010).
28. B. D. Barmashenko and S. Rosenwaks, "Detailed analysis of kinetic and fluid dynamic processes in diode-pumped alkali lasers," J. Opt. Soc. Am. B **30**, 1118-1126 (2013).